NJC

Accepted Manuscript

This is an *Accepted Manuscript*, which has been through the Royal Society of Chemistry peer review process and has been accepted for publication.

Accepted Manuscripts are published online shortly after acceptance, before technical editing, formatting and proof reading. Using this free service, authors can make their results available to the community, in citable form, before we publish the edited article. We will replace this *Accepted Manuscript* with the edited and formatted *Advance Article* as soon as it is available.

You can find more information about *Accepted Manuscripts* in the Information for Authors.

Please note that technical editing may introduce minor changes to the text and/or graphics, which may alter content. The journal's standard Terms & Conditions and the Ethical guidelines still apply. In no event shall the Royal Society of Chemistry be held responsible for any errors or omissions in this *Accepted Manuscript* or any consequences arising from the use of any information it contains.

ROYAL SOCIETY OF CHEMISTRY

www.rsc.org/njc

Please do not adjust margins

ARTICLE NJC

Multi-nuclear NMR of axially chiral biaryls in polypeptide orienting solvents: spectral discriminations and enantiorecognition mechanisms

Received 00th June 2015,
Accepted 00th ***2015

DOI: 10.1039/x0xx00000x

www.rsc.org/

Philippe Berdagué,[a] Jose-Enrique Herbert-Pucheta,[a] Vishwajeet Jha,[b] Armen Panossian,[b] Frédéric R. Leroux,[b] and Philippe Lesot[a]*

Due to the importance of axially chiral biaryl derivatives as chiral auxiliaries and/or ligands for asymmetric synthesis as well as their structural role in bioactive natural products, continuous efforts have been undertaken to propose efficient methods for their atropo-selective synthesis. As a consequence, proposing robust and reliable analytical tools able to discriminate the signal of atropisomeric enantiomers becomes crucial to evaluate the enantiomeric excesses of mixtures. In this work, we show how several multi-nuclear 1D/2D-NMR techniques using homopolypeptide chiral liquid crystals as aligning solvents can provide a panel of analytical possibilities (through differences of chemical shift anisotropies, dipolar and quadrupolar residual couplings) to spectrally discriminate enantiomers of a large collection of trisubstituted axially chiral biphenyls. Approaches involving ^{31}P, ^{13}C and ^{2}H 1D- or 2D-NMR experiments at natural abundance level are explored. Among noteworthy results, the first examples of spectral enantioseparations using ^{31}P nuclei as nuclear probe are reported. Finally, the role of electronic factors and shape anisotropy that affects the efficiency of chiral discrimination mechanisms are examined and discussed. Molecular modeling calculations were carried out to establish the electronic profile of these analytes in order to understand and rationalize the ^{13}C-{^{1}H} NMR results.

Introduction

Axially chiral biaryl derivatives possess a peculiar stereochemical motif able to generate a couple of stereoisomers. The stereogenic structural motif is present in various potentially bioactive natural compounds and exhibits a wide range of biological properties.[1] For instance, one can mention the well-known Vancomycin (a clinically used antibiotic glycopeptide)[2] or Steganacin (a cytotoxic tubulin-binding dibenzocyclooctadiene lignan).[3] In fact, the biaryl scaffold belongs to the privileged structures for pharmaceutical research as its incorporation assures frequently high entry rates.[4] In addition, the stereogenic axes provide rigid molecular frameworks for highly efficient tools in asymmetric synthesis.[5] Concomitantly, atropisomeric C_1-symmetric biaryls play an important and effective role as chiral auxiliaries and/or ligands for asymmetric synthesis. Consequently, continuous efforts have been undertaken by organic chemists to develop efficient methods for the atropo-selective synthesis of ligands based on the biphenyl, binaphthyl, or other biaryl backbones.[6] The conformational stability of bridged biaryls can be strongly increased by incorporation of *ortho*-substituents, the associated rotational energy barrier primary depending on the number and bulkiness of those substituents.[7] Generally, *ortho*-trisubstituted biphenyls show no stereo-labile properties, and hence no rapid enantiomerization at room temperature is expected (see **Figure 1a**).[8]

So far, both chiral supercritical fluid chromatography and chiral gas chromatography were the main methods to separate the enantiomers of such peculiar chiral compounds.[8,9] Although adequate in numerous cases, chromatographic approaches present some well-known specific drawbacks for its systematic implementation (price of chiral columns, for instance). Furthermore, the determination of experimental conditions leading to enantiomeric resolution is sometimes highly time-consuming. As a consequence, proposing (simple) analytical alternatives involving other techniques as NMR spectroscopy to chemists is a valuable task.

In the past, liquid-state NMR methods involving mainly chiral derivatizing agents (MPTA or Mosher's acid) in combination with or without lanthanide shift reagents have been proposed to discriminate enantiomers of (bridged or not) chiral biaryl atropisomers.[10] Although successful, these approaches require the presence of accessible reactive groups (-COOH, -OH, -NH_2, …) to generate (*in situ* or not) diastereoisomers.

Overcoming of this prerequisite can be found when using NMR in lyotropic chiral liquid crystals (CLC). This breakthrough approach revealed to be a powerful and flexible tool, providing a robust and general alternative to the multitude of isotropic NMR methods for the differentiation of enantiomers of chiral molecules,[11] but also enantiotopic elements in prochiral molecules.[12,13,14] Compared to classical NMR approaches using chiral derivatizing or solvating chiral agents, NMR in CLC requests no specific functional groups inside the analyte[15] while all magnetically active nuclei (even at very low natural abundance level) can provide effective probes.

Using a chiral aligned environment, the intermolecular interactions between each enantiomer (or each enantiotopic

[a] *Laboratoire de RMN en Milieu Orienté, Université Paris-Sud, Institut de Chimie Moléculaire et des Matériaux d'Orsay (ICMMO), UMR CNRS 8182, 91405 Orsay, France. E-mail : philippe.lesot@u-psud.fr ; Tel.: +33 (0)1 69 15 47 59; Fax : +33 (0)1 69 15 81 05*

[b] *Laboratoire de Chimie Moléculaire, Université de Strasbourg, UMR CNRS 7509, ECPM, 25 Rue Becquerel, 67087 Strasbourg, France.*

† Electronic Supplementary Information (ESI) available: A description of experimental details and DFT calculation, analytical details, chemical pathway, background of NMR in CLC, further 1D/2D NMR spectra, and NMR assignment data of compound 16 are given.
See DOI: 10.1039/x0xx00000x

New Journal of Chemistry Accepted Manuscript

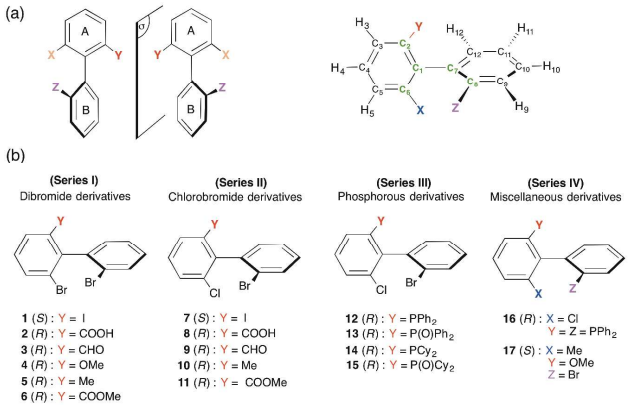

Fig. 1: (a) General structure of enantiomeric couples of *ortho*-trisubstituted biphenyls investigated here, along with the systematic atomic numbering used. The aromatic cycle B contains the Z substituent and quaternary carbon atoms are displayed in green. (b) Structures of chiral compounds **1** to **17** defined by series: (I): dibromo derivatives (**1** to **6**); (II): chloro-bromo derivatives (**7** to **11**); (III): monophosphorous derivatives (**12** to **15**); (IV): miscellaneous derivatives (**16** and **17**). The stereodescriptors reported in the four series correspond to structures drawn. As short notation associated to atropisomers, we will use the stereodescriptors (*S*/*R*) instead of (a*S*/a*R*).

direction) and the CLC differ, and hence the internuclear vectors, i-j, are not oriented the same on average, $S^{S}_{i-j} \neq S^{R}_{i-j}$ (or $S^{\text{pro-}S}_{i-j} \neq S^{\text{pro-}R}_{i-j}$).[11,12,13] A doubling of the spectral information/patterns for a given nuclear site indicates therefore that the enantiorecognition phenomenon occurs and is revealed on the NMR spectrum by a difference of residual chemical shift anisotropies (CSA), dipolar couplings (D) or quadrupolar couplings ($\Delta\nu_Q$) (for spin I > 1/2) (see **Figure SI-1**).[16,17] As first example, deuterium NMR in CLC was used to analyze the intramolecular dynamic processes of chiral and prochiral deuterated *ortho*-disubstituted biaryls (derivatives of 1-(4-methylphenyl)naphthalene).[14]

In this work, we show how multi-nuclear 1D/2D-NMR using chiral anisotropic solvents (homopolypeptide CLC) can provide various analytical possibilities to spectrally separate enantiomers of a large collection of *ortho*-trisubstituted axially chiral biphenyls (see **Figure 1**). From an analytical viewpoint, anisotropic NMR results will be discussed in terms of spectral enantiodiscrimination efficiency and an attempt of rationalization of results will be proposed. For this purpose, the seventeen analytes investigated have been classified into four series of structurally related molecules (**I** to **IV**) depending on the similarity of their substitution patterns as displayed in **Figure 1b**.

Experimental section

Synthesis

The synthesis of these atropisomeric biaryls was recently reported using an original, modular approach (see **Figure SI-2**).[8] Briefly speaking, it is based on (a) the preparation of *ortho,ortho'*-dibromobiphenyls bearing an additional substituent in the 6-position *via* a transition metal-free aryl-aryl coupling -the 'ARYNE coupling'-,[18] (b) the regioselective introduction of an enantiopure *p*-tolylsulfinyl group as traceless chiral auxiliary allowing the separation of atropo-diastereoisomers by simple crystallization, (c) the chemoselective functionalization of this auxiliary and (d) subsequent regioselective functionalization of the remaining bromine atoms. During all these chemical transformations, the configuration of the biaryl axis is maintained, and hence no racemization was found to occur.[8] The diphosphine **16** was obtained by means of catalytic C-P coupling.[19]

Material for oriented NMR samples

In this study, homopolypeptide CLC samples were made of poly-γ-benzyl-L-glutamate (PBLG), purchased from Sigma and dissolved in chloroform.[11,20] The degree of polymerization of PBLG is equal to 743 (MW = 162 900 g/mol). The mass of solute in samples varies from 19 to 100 mg, while the molar variation ranking from 2.1 10^{-6} (sample **14**) to 1.8 10^{-4} mol *per* enantiomer (sample **17**). **Table SI-1** lists the exact composition (samples **1** to **17**) and if the chloroform was protonated or deuterated. The preparation of (sealed) anisotropic NMR tubes and practical aspects have been reported in previous papers (see ESI, also).[10,12,13]

NMR spectroscopy

^{13}C, ^{13}C-{^{1}H} and ^{31}P-{^{1}H} 1D/2D-NMR spectra were recorded on routine 9.4 T Bruker (Avance I) NMR spectrometers equipped by either of a 5-mm BBO, TBI or QXO probe. Without otherwise specified, the sample temperature was set to 298 K. NAD-{^{1}H} 2D NMR spectra were performed on 14.1 T Bruker (Avance II) spectrometer equipped by a 5 mm ^{2}H selective cryoprobe,[17,21] WALTZ-16 CPD sequence has been used to decoupled proton (0.5 W).[11] Specific experimental details are given in figure captions.

Molecular modeling and DFT calculations

Geometry optimizations and electronic structure determinations were carried out using the Gaussian 09 program running on the "IDA" cluster of University of Paris-Sud.[22] Density Functional Theory (DFT) with Self-Consistent Reaction Field (SCRF) Tomasi's Polarized Continuum Model (PCM) for solvation[23] was used in all calculations to describe implicitly the solvent (chloroform) for energy minimizations and description of orbitals. All computations were performed with the hybrid method B3LYP, whereas electronic correlation and exchange were respectively described by the use of the Becke[24] and Lee-Yang-Parr[25] functionals. Relativistic effective core potentials (ECP) were used to describe electrons of heavy atoms (Br and Cl) with the valence double z quality basis sets Lanl2dz.[26] The standard 6-311G(d,p) basis sets were used for the rest of the atomic orbitals' descriptions of H, C, O and P atoms. Local minima conditions *per* molecule were confirmed with the calculation of harmonic vibrational frequencies of all structures. None of the predicted vibrational spectra has any imaginary frequency (data not shown), implying that the optimized geometry of each of the molecules under study lay at a local point on the potential energy surface. The electronic properties such as Molecular Electrostatic Potential (MEP), frontier molecular HOMO-LUMO orbital energies and Mulliken atomic charges have been obtained with the same level of theory as previously described.

New Journal of Chemistry Accepted Manuscript

 This journal is © The Royal Society of Chemistry and the Centre National de la Recherche Scientifique 2015

Please do not adjust margins

Table 1: Compilation of various solute parameters and the associated number of discriminated sites (racemic series) using proton-decoupled ^{2}H, ^{13}C and ^{31}P NMR results in PBLG

Series	Solute	Mass (mg)	10^{-5}x$n^{R\text{ or }S}$ /mole	μ_{mol}(scalar) /D[g]	Hydrogen bond	Oxygen atom	^{13}C-{^{1}H} NMR	^{2}H-{^{1}H} NMR	^{31}P-{^{1}H} NMR
I (Br/Br)	**1** (I)	19.9	2.27	2.132	N	N	1 / 12[b]	/[c]	-
	2 (COOH)	54.5	7.65	2.529	Y	Y	12 / 13	US[e]	-
	3 (CHO)	61.0	9.00	2.933	N	Y	9 / 13	7 / 8[f]	-
	4 (OMe)	100.0	14.60	4.213	N	Y	10 / 13	7 / 8[f]	-
	5 (Me)	21.2	3.25	3.104	N	N	6 / 13	NS	-
	6 (COOMe)	72.2	9.75	2.963	N	Y	8 / 13	6 / 8	-
II (Cl/Br)	**7** (I)	21.1	2.68	2.213	N	N	3 / 12	/	-
	8 (COOH)	59.5	9.55	2.357	Y	Y	11 / 13	US[e]	-
	9 (CHO)	62.6	10.60	2.737	N	Y	11 / 13	6 /8[f]	-
	10 (Me)	19.0	3.38	3.179	N	Y	6 / 13	NS	-
	11(COOMe)	70.1	10.75	3.006	N	Y	8 /13	6 / 8	-
III (Cl/Br)	**12** (PPh_2)	26.0	2.88	4.166	N	N	4 / 24[d]	/	0 / 1
	13($POPh_2$)	96.2	10.26	4.622	N	Y	12 / 24[d]	/	0 / 1
	14 (PCy_2)	25.3	2.73	3.048	N	N	3 / 24[d]	/	1 / 1
	15 ($POCy_2$)	20.1	2.09	5.146	N	Y	2 / 24[d]	/	0 /1
IV	**16** (P_2)[e]	30.4	2.73	5.290	N	N	12 / 36[d]	/	2 / 2
	17(Me/OMe)	100.6	18.20	2.377	N	N	6 / 14	7 / 9[f]	-

[a] Y : Spectral discriminations observed. In parenthesis are given the number of ^{13}C sites discriminated. [b] N : Spectral discrimination not observed. [c] / : Spectrum not recorded. [d] ^{13}C signals are also decoupled from ^{31}P signals. [e] US : Unexpoitable NAD spectrum. [f] For one site ^{2}H, two interpretations of results are possible. [g] The molecular electric dipole moment, μ_{mol}, is calculated for the lowest-energy conformer.

Results and Discussion

For a global view of results, **Table 1** (see also **Table SI-2**) summarizes the essential data of analytes and the sets of

experimental results. As all results were obtained with very similar experimental conditions (T ≈ 298 K, W/W of PBLG of 14%), we will then follow with their interpretation in terms of chiral discrimination mechanisms (noted in short CDMs). In particular, ^{13}C NMR results, attempts to correlate the number of discriminated sites (NDS (^{13}C) and the possible solute-PBLG electrostatic interactions in combination with molecular shape recognition effects will be proposed and discussed.

^{1}H 1D-NMR spectroscopy

Even for small-size molecules, the number and the magnitude of (short and long-range) ^{1}H-^{1}H residual dipolar couplings increase significantly the linewidth up to obtain rather low-resolution ^{1}H spectra where no fine structures clearly emerge. Some exceptions can be found with molecules possessing isolated methyl groups, for instance. Compounds **4** to **6**, **10, 11** and **17** are typical examples. Contrarily to isotropic ^{1}H NMR, an uncoupled methyl group exhibits a triplet structure in a LC (instead of a single resonance) due to the intramethyl ^{1}H-^{1}H dipolar couplings (see **Figure SI-3**). In a CLC, two triplets with different splittings ($\left|3D^{S}_{HH}\right| \neq \left|3D^{R}_{HH}\right|$) centered on very close ^{1}H chemical shifts (due to a small difference of ^{1}H CSA) are generally detected.

For analytes, **6** and **11**, a single triplet (with $|3D_{HH}|$ = 58 and 52 Hz, respectively) is observed, thus revealing no resolved discrimination through a difference of D_{HH}. Two reasons may explain this absence of enantiodiscriminations: i) the rather low sensitivity of $D(^{1}H$-$^{1}H)$ to a difference of orientational ordering (compared to ^{2}H quadrupolar interaction, for instance); ii) the complex conformational dynamics of ligand Y (here, up to three rotors) that generally leads to average down the order parameters of each internuclear vector along the chain, and subsequently reduce spectral enantiodifferences. For solutes **5**, **10** and **17**, a symmetric ^{1}H spectral pattern of six lines are observed for methyl bounded to ring (see **Figure SI-3**). This structure can be analyzed as following: i) a dedoubled triplet if methyl group is dipolarly coupled with one of the aromatic protons; ii) two triplets centered on two ^{1}H chemical shifts due to a surprisingly large ^{1}H CSA. Two approaches involving the components of mixture can be proposed to assess the origin of spectral pattern. They consist into either recording the ^{1}H spectrum in ALC made of a racemic mixture of PBLG and PBDG (PBLG's enantiomer)[27] or using the enantiopure compound (when available) in the CLC. Irrespective the method used, it appears here that the doubling of triplets has its origin from the dipolar coupling with the *ortho*-position aromatic proton as simply exemplified in case of **10** (see **Figure SI-1**). Spin-manipulation based alternatives for simplifying the coupling pattern of ^{1}H signals should be possible but they are over the scope of this paper and have been not explored.

^{1}H-(de)coupled ^{31}P NMR spectroscopy.

Compounds **12** to **16** possess ^{31}P nuclei that are both sensitive and 100% abundant, and hence easy to detect. Spectral enantiodisciminations can be observed through a difference of ^{31}P CSA, leading to two independent resonances, one for each enantiomer, or a difference of ^{31}P-^{1}H RDCs. For the series of monophosphorous derivatives, no exploitable spectral separations based on ^{31}P-^{1}H RDC differences were obtained on the ^{31}P 1D spectra, mainly due to the presence of various long-range ^{31}P-^{1}H RDCs that obscure spectra. When protons are decoupled, spectra are significantly simplified. Contrarily to **12, 13** and **15,** the presence of two ^{31}P resonances for solute **14** indicates that

New Journal of Chemistry Accepted Manuscript

enantiomers are discriminated on the basis of ^{31}P CSA differences ($|\Delta\sigma|$ = 14 Hz, $\Delta\nu_{1/2}$ = 3.5 Hz) (see **Figure 2a**). Surprisingly, monophosphine oxide biaryl moieties **13** and **15** are not spectrally discriminated even though the expected increase of the electronic shielding anisotropy of phosphorous nuclei due to the presence of the oxygen atom that produces important differences in the ^{31}P CSA that would allow successful enantiodiscrimination. Variable temperature ^{31}P NMR experiments (range of 30 K) did not permit enantiodiscriminations neither for **13** nor for **15**. The last strongly suggest that the energy gap of the interconversion barrier between enantiomers is importantly increased by the fact that aryls' free-rotation is sterically hindered by the presence of the oxide and thus only one enantiomer is favored.

Finally, the case of chiral biaryl-based diphosphane **16** is rather peculiar. Indeed in liquid state, this molecule possesses two anisochronous ^{31}P atoms (at room temperature) resonating at two distinct chemical shifts ($\delta^{31}P_A$) = -12.0 ppm and $\delta^{31}P_B$) = -14.1 ppm) and mutually coupled as first evidenced in 2011.[28] This spin-spin coupling finds its origin via a "through-space" scalar coupling (noted $J(^{31}P_A\text{-}^{31}P_B)$ = 22.7 Hz) and not via the intramolecular five-bond connectivity that should lead to a small scalar $^5J(^{31}P_A\text{-}^{31}P_B)$ coupling. The spectral assignments of P_A and P_B atoms derive from the analysis of ^{1}H-^{31}P 2D HMBC, ^{31}P 2D J-resolved and ^{1}H-^{1}H 2D COSY experiments shown in **ESI** (**Section III**). If two doublets (AX spin system) are observed on the isotropic ^{31}P-{^{1}H} spectrum, four resonances ($\Delta\nu_{1/2}$ < 0.8 Hz) are detected at each ^{31}P site in racemic series (see **Figures SI-2a** and **SI-4**). This doubling of lines indicates enantiodiscrimination. Three spectral situations corresponding to a difference of either ^{31}P CSA or ^{31}P-^{31}P RDC or from both contributions can explain the presence of two pairs of doublets for each ^{31}P site (see **Figure SI-5**). The assignment of ^{31}P resonances, has been assessed by comparing the 1D spectrum of **16** to the one recorded with an enantioenriched mixture (enriched in *R* isomer, *ee* = 51.3 %) using similar experimental conditions (sample composition and temperature). As seen in **Figure 2b**, the peak intensity difference between enantiomers allows their associated signals to be undoubtedly assigned. Various homonuclear 2D experiments confirm qualitatively the presence of each enantiomer, regardless the absolute configuration of NMR signals (*vide infra* and ESI). Accordingly to the enantio-assignment made, the analysis of ^{31}P-{^{1}H} 1D spectrum of **16** indicates that total couplings between the two ^{31}P nuclei for each isomer, $|T^A(^{31}P\text{-}^{31}P)|$ and $|T^B(^{31}P\text{-}^{31}P)|$ with T = J + 2D are very close and equal to 18.7 and 19.1 Hz, respectively while each doublet is shifted of 3.9 Hz ($^{31}P_A$) and 4.5 Hz ($^{31}P_B$). Assuming a negative value for $T^{A\ or\ B}$, the magnitude of $D(^{31}P\text{-}^{31}P)$ is equal to -20.3 and -20.5 Hz for *R* and *S*. Conversely, if $T(^{31}P\text{-}^{31}P)^{A\ or\ B}$ is positive, $D(^{31}P\text{-}^{31}P)^{A\ or\ B}$ becomes equal to -2 or -1.8 Hz, respectively. Among the two anisotropic contributions (D and CSA), only the ^{31}P CSA ($\Delta\Delta\sigma$ = 3.9 Hz and 4.5 Hz) is the relevant NMR interaction here that can be *in fine* efficiently exploited to evaluate the *ee*. As CSA is directly proportional to the magnetic field strength, operating with higher magnetic field spectrometers should guarantee larger discriminations. Interestingly, the results obtained here are the two first examples of enantiodifferentiation using ^{31}P-{^{1}H} NMR, so far. Previous studies using ^{31}P-{^{1}H} or ^{31}P NMR as analytical technique had failed in discriminating enantiomers of phosphorous compounds.[29]

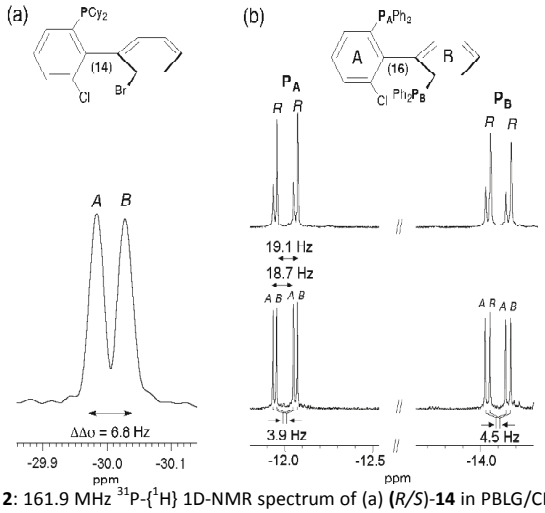

Fig. 2: 161.9 MHz ^{31}P-{^{1}H} 1D-NMR spectrum of (a) **(*R/S*)-14** in PBLG/$CHCl_3$ at 335 K and (b) of **16** in racemic series (bottom) and enantioenriched series (*R* isomer) (top) in PBLG/$CDCl_3$ at 298 K (ref. (80 % of H_3PO_4) = 0 ppm). 1000 scans (a) and 5000 scans (b) are added and soft line-sharpened Gaussian filtering is applied. Note the ^{31}P CSA of 3.9 Hz and 4.5 Hz for P_A and P_B of **16**. The assignment of P_A and P_B atoms is given in ESI (see **Figures SI-14** to **SI-18** in **Section SI-III**). The italicized notations "*A*/*B*" stand for the chiral stereodescriptors of enantiomers *A* and *B*.

^{1}H-decoupled ^{13}C 1D-NMR

Although basically less sensitive compared to ^{1}H or ^{31}P NMR, the anisotropic ^{13}C-{^{1}H} NMR at natural abundance is an excellent and competitive method to discriminate enantiomers in particular when sp^2 hybridized carbon atoms are present in the analyte. The gain in sensitivity of commercially available cryogenic probes with respect to conventional ones (up to a factor of 4 to 5) enables reducing the experimental acquisition times of qualitative ^{13}C-{^{1}H} NMR to less than 1-2 hour(s),[30] even working with small amounts of solutes or with analytes of high MW. However, when a sufficient amount of solute is available (10-30 mg), depending on the enantiomeric mole number (from 2.27×10^{-5} to 18.20×10^{-5}) and the S/N ratio (SNR) desired, all ^{13}C-{^{1}H} 1D spectra were recorded with a moderate magnetic field (9.4 T) using acquisition times in the range of 3 – 10 hours.

All experimental data related to the number of discriminated ^{13}C sites in PBLG are presented in **Table 1**, while **Table SI-3** lists the value of all $\delta(^{13}C)$ and the differences of CSA ($\Delta\Delta\sigma$) for each of them.

For derivatives of series **I** and **II**, the 1D analysis of ^{13}C-{^{1}H} NMR spectra in CLC can be easily performed by counting the number of ^{13}C lines and then comparing with the isotropic ^{13}C-{^{1}H} NMR spectra where no discrimination occurs (see **Figure SI-6**). For all of them, several spectral enantiodiscriminations occur both in the CH and quaternary aromatic carbon atoms, but the number of differentiated ^{13}C sites varies from one (solute **1**) to twelve sites (solute **2**), with spectral difference from 1 Hz (limit of discrimination) to 14 Hz. Note that carbon atoms belonging to the Y substituent (see **Figure 1**) can provide further potential ^{13}C sites for discrimination like in the case of **4**, **9** and **10**, for instance (see **Table SI-3**).

New Journal of Chemistry Accepted Manuscript

 This journal is © The Royal Society of Chemistry and the Centre National de la Recherche Scientifique 2015

Two illustrative examples of ^{13}C-{^{1}H} 1D spectra (solutes **2** and **8**) are given in **Figure 3**. The variations of $\delta(^{13}C)$ between **2** and **8** (and between each solute) result in the well-known electronic effects (+I, -I and +M, -M) of various substituents on the rings (see also **Figure SI-4**). For **2** and **8**, about 90% of ^{13}C sites are discriminated, thus affording a multiple choice for measuring *ee*'s However, from a quantitative viewpoint, the choice of the best sites is clearly governed by three parameters i) the spectral frequency differences between enantiomer signals; ii) SNR, iii) signal overlapping of analytes with solvent signals. Typically, for **2** and **8**, the C-4 atom (SNR ≈ 80-100) provides the best site for quantitative purposes when the PBLG/$CHCl_3$ chiral system is used. Carbon atom C-9 could also provide a discrimination site but the signal overlay with very broad resonances of PBLG aromatic signals complicates the evaluation of enantiomeric purity. Finally the quaternary C-6 and C-8 (for **2**) or C-6 (for **8**) carbons provide also large separations (≈ 11 Hz), but their low SNR (≈ 30-35) excludes them for the accurate measurement of large *ee*'s. The overall interspectral analysis of all analytes indicates that biaryls with an aldehyde (**3** and **9**), ether (**4**) and ester (**6** and **11**) substituent possess numerous enantiodiscriminated sites (60 to 80%) but these sites show smaller spectral differences (1 to 3.5 Hz).

For methylated biaryls (**5** and **10**), the ratio of enantiodiscriminated sites does not exceed 50% while the lowest number of sites (<25%) is obtained for the iodo derivatives (**1** and **7**). ^{13}C-{^{1}H} 1D-NMR spectra of **7** and **9** are given in ESI. Similar experimental conditions (co-solvent, w/w of polypeptide and temperature) for all solutes allow ^{13}C spectral comparisons. Furthermore, the ^{13}C CSA is weakly sensitive to small variations of T or sample concentration.

Due to the diversity of contributing factors/effects to the CDMs (molecular shape, electronic properties and/or conformational dynamics), the attempt to establish qualitative correlations between the enantiodiscrimination efficiency and molecular properties are far to be trivial. Nevertheless, it is important to investigate them in order to rank their role and evaluate their respective predominance contributing to the CDMs. This is a prerequisite step toward a global insight of the phenomenon, and subsequently the possibility to predict spectral results for any given analyte.

Considering the rather high degree of structural homology (*ortho*-three-substituted biaryl) of analytes in series **I** and **II**, we have first attempted to simply correlate (and explain) the ^{13}C NDS and the range of spectral separations ($\Delta\Delta\sigma(^{13}C)$) (weak (1-3 Hz), medium (4-8 Hz) or large (> 9 Hz)) to the magnitude of the global dipolar moment, μ, of the molecule calculated by molecular modeling. For this purpose, the dipole moments (in $CHCl_3$) for all biaryls in their lowest-energy conformation have been calculated using solvent-dependent Density Functional Theory (SCRF-DFT) Mulliken charge distribution analysis (see Exp. Section for details). The scalar value, the three-axis components (x,y,z) and their vectorial representation are given in **Table SI-4**. A first inspection of molecular modelling results shows that: i) the variation of μ does not exceed 7 % when Br is replaced by the chlorine atom; ii) the nature of substituent Y modifies significantly the value of μ, from 2.1 (**1**) to 4.2 D (**4**).

The comparison of NMR results between series **I** and **II** shows rather similar results (NDS and $\Delta\Delta\sigma$), thus indicating, that the replacement of Br by Cl atom in position 6 (ring A) do not modify significantly the global molecular (dipole moment and shape) properties of solute towards the efficiency of CDMs. In contrast, in each series, the difference of properties of ligand Y has a larger impact on both criteria. Except for solutes **1** and **7** which both exhibit the smallest values of μ and NDS (with small $\Delta\Delta\sigma$), the analysis of results for other analytes indicates that there is no simple dependency (i.e. a monotonous variation) between both spectral criteria and the magnitude of global dipole moment. In clear, the larger NDS does not occur for the biggest μ. This absence of direct correlation suggests that the nature of substituent Y and the associated specific electronic properties (presence of labile hydrogens able to form intermolecular hydrogen bondings (HB) or the presence of electronegative oxygen in carbon-oxygen double bond, for instance) play a crucial role in the efficiency of CDM for this series of biaryls, independently to the molecular dipole moment. Thus the best results obtained with acid derivatives **2** and **8**, and not for the methyl ester analogues (**6** and **11**), point out that the possibility of forming HB between the substituent Y and the oxygen of the carboxylate group of the PBLG side chain is of primary importance in the CDM. Schematically, the role of HB can be understood as follows. Contrarily to ordering mechanisms (mainly due to the coupling between the solute quadrupole moment and the electric field gradient of the solvent), the CDMs involve short-range intermolecular interactions that derive from the repulsive forces correlated with the size and shape (and the shape-anisotropy) of the solute.[31] Hence the CDM efficiency is strongly dependent on the average distance between the solute and the PBLG chiral helix. In this context, irrespective of the magnitude of the global dipole moment, HB can be seen as crucial local electronic interaction susceptible to bring closer the solute at small distances to the fibers, thus promoting in turn better enantiodiscriminations, this effect being particularly strong when the labile hydrogen is highly topologically accessible as in case of **2** and **8**.

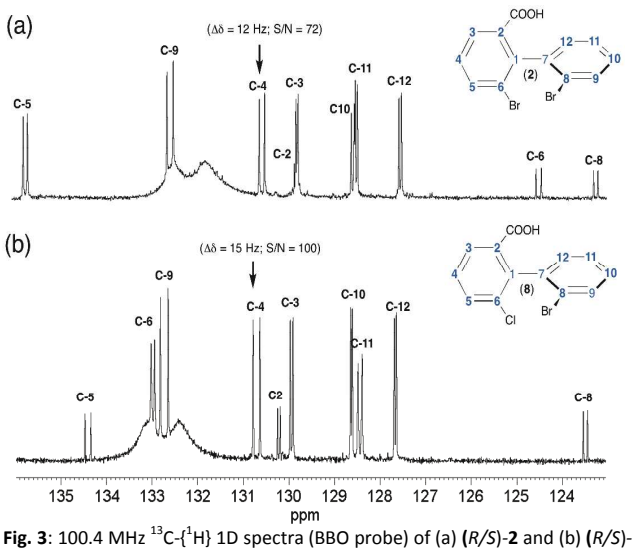

Fig. 3: 100.4 MHz ^{13}C-{^{1}H} 1D spectra (BBO probe) of (a) **(***R/S***)-2** and (b) **(***R/S***)-8** recorded in PBLG/$CHCl_3$. Only the region ranging from 123 and 136 ppm is displayed (carbons C-1/C-7 and from carboxyl group not shown). Note the doubling of numerous ^{13}C signals (compared to isotropic spectra) associated to the spectral discrimination of *R/S* isomers. The very broad resonances observed around 132-134 ppm originate from *ortho*/*meta* aromatic signals of the benzyl group of the PBLG side chain.

New Journal of Chemistry Accepted Manuscript

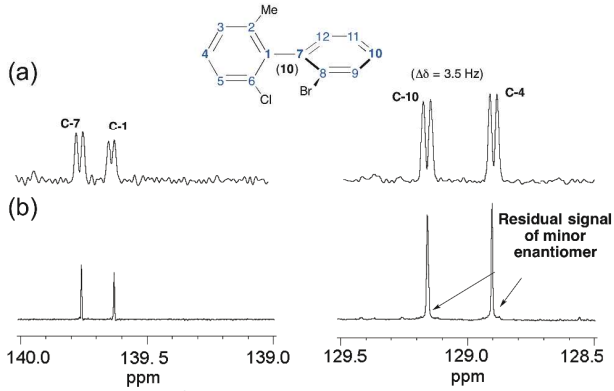

Fig. 4: Comparison of ^{13}C-{^{1}H} 1D signals of carbons C-1, C-4, C-7 and C-10 of **10** in (a) racemic and (b) enantiopure series (*R*) recorded with 4 k and 8 k scans added, respectively. For those four sites, enantiodiscrimination is observed. The *ee* measured is about 95 %.

When no HB are possible, other attractive specific electronic interactions can play important roles in the CDM, in particular to reduce the average solute-PBLG distance. Although probably less efficient than HB, these (secondary) interactions become then key parameters governing the efficiency of discrimination. Clearly the presence of an electronegative oxygen atom with accessible lone pairs (aldehydic or ester groups for instance) appears as an important electronic parameter favoring fiber-solute electrostatic interactions (van der Waals type). In contrast (*vide infra*), it is *a priori* expected that CDM are much less efficient for biaryls devoid of any groups susceptible to promote any attractive intramolecular interactions (case **5** and **10**). This simply explains why better results are obtained for methoxy, carbonyl or ester groups (NDS varying from 8/13 to 10/13), whereas the situation is much less favorable for methyl (NDS = 6/13). From the spectral enantiodiscrimination viewpoint, the case of methoxy or aldehydic derivatives (**3**, **4**, **9**, **17**) could be qualified of "intermediate" situation for which only enantiodiscriminations with moderate spectral differences are expected and occur.

As an illustrative example of the experimental quantification of *ee*'s of enantioenriched chiral biaryl mixtures, **Figure 4** compares the signals of four ^{13}C sites of **10** in racemic (top) and enantioenriched mixtures (*R*) (bottom). Thus, in enantioenriched series, a single resonance is observed at quaternary carbons (C-1 and C-7) for which the SNR is smaller (137 and 114) compared to *para* methine sites (C-4 and C-10) (SNR = 317 and 375). In contrast for the latter case, a very weak signal can be found at the foot of the most intense ^{13}C signal, indicating that the mixture is not enantiopure but only enantioenriched (see **Figure 7b**, **right panel**). Evaluation of peak areas by deconvolution indicates an *ee* of about95 % (in good agreement with the chromatographic results)[8], while the absence of signals for the minor enantiomer at quaternary carbon atoms (C-1 and C-7) could suggest an *ee* = 100%. This example points out the importance of sites selected for quantitative measurement, in particular when a reliable evaluation of *ee* is necessary. The analysis of ^{13}C-{^{1}H} spectra of molecules of Series **IV** is analytically much more challenging for two reasons: i) the important number of sp^2 carbon atoms (up to 24 sites) in the aromatic region ranging from 123 to 145 ppm (**12** and **13**); ii) the weak distribution of chemical shifts of sp^3 carbon atoms in aliphatic region (from 25 to 34 ppm) of cyclohexyl rings (**14** and **15**). For all phosphorous analytes, the determination of $\delta(^{13}C)$ listed here was achieved from the analysis and the intercomparison of ^{13}C-{^{1}H} and ^{13}C-{^{1}H, ^{31}P} 1D-NMR spectra and ^{13}C-{^{1}H} and ^{13}C-{^{1}H, ^{31}P} J-modulated 1D-NMR spectra. All $\delta(^{13}C)$ measured (and the associated $|\Delta\Delta\sigma|$) at 9.4 T are reported in **Table SI-3**. Globally, the results from the ^{13}C enantiodiscrimination side are rather mediocre and disappointing because only very few carbon sites (with tiny spectral differences) show useful separation both in phenyl and cyclohexyl rings. Actually two reasons may explain the absence of numerous and large differentiations. The first one is related to the presence of sp^3 carbon atoms in cyclohexyl groups (**14** and **15**), which are less susceptible to be discriminated on basis of ^{13}C chemical shift anisotropy (spherical electronic screening). The second one could originate from the global shape of the molecule. Indeed the presence of biphenylphosphine (oxide or not) moiety significantly increases the size of the structure (four cycles), and concomitantly leads to a more globular molecular topology (regardless of the conformational dynamics). In a simple (static) schematic view, increasing of the number of (aromatic or aliphatic) cycles reduces the geometrical shape anisotropy (compared to molecules of series **I** and **II**), and in turn the efficiency of shape recognition mechanisms that are also another key parameter in the CDM.[17a] To illustrate this idea, **Figure 5** shows the electronic topologies of **3** and **12** displayed in terms of the DFT-computed electrostatic potential contour plots associated to the optimized electronic structures. As seen, the surfaces for these two examples significantly differ from each other. Thus solute **3** shows a rather cylindrical topology (with a diameter (D) of about 8 Å and a length(L) of about 11 Å, leading to a D/L ratio of 0.72) whereas **12** has a roughly spherical topology (with D ≈ 15 Å). Actually the former one is representative of the topology (rod-like type) adopted by biaryls of series **I** and **II** (including also **17** of series **IV**) which D/L ratios differ accordingly with the nature of the X and Z substituents. In contrast, the latter schemes the typical topology (rather spherical shape) of series **III** (including also analyte **16** of series **IV**) which D varies between 15 and 18 Å (see **Table SI-4**). Reasonably, the shape recognition mechanisms where the topological anisotropy plays a substantial role are expected to be less efficient in the second case.

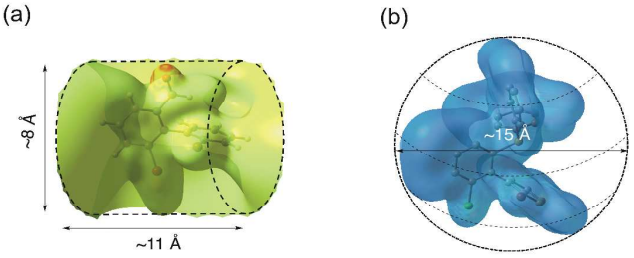

Fig. 5: Two examples of electrostatic potential (ESP) surfaces (by plotting only their positive contribution and restraining the contour level with isovalues of 0.005 a. u. for both cases) associated to (a) **3** and (b) **12**.

New Journal of Chemistry Accepted Manuscript

This journal is © The Royal Society of Chemistry and the Centre National de la Recherche Scientifique 2015

^{1}-H-coupled ^{13}C 1D-NMR

At a first glance, and compared to ^{13}C-{^{1}H} NMR in CLC, ^{13}C NMR might be seen of limited practical interest for two reasons: i) the complexity of spectral pattern due to the presence of both short range ($^{1}D_{CH}$) and long range ($^{n}D_{CH}$, n = 2,3) RDCs; ii) the distribution of ^{13}C signals on numerous lines, thus reducing the SNR, and hence the accuracy on the *ee*. However, this approach must be kept in the panel of tools because it can also provide a solution to reveal chiral discriminations. In particular, it can reveal as a useful alternative to ^{13}C-{^{1}H} NMR when molecules possess few or none sp, sp^{2} carbon atoms. Besides, using simple heteronuclear 2D-NMR experiments (see below), it becomes possible to simplify the spectral analysis of fine ^{13}C-^{1}H structures, while the measurement of peak volumes on 2D maps allows to determine the *ee* when the signal of each enantiomer has been identified.

Another potential source of useful information can be found out from the analysis of ^{13}C signals of substituent Y (see **Figure 1**) in particular when small (isolated) groups such as methyl or methoxy are present. Indeed such moieties can lead to very simple spectral patterns to analyze since they are primarily governed by direct $^{1}D_{CH}$, that in turn gives rise to quadruplet structures (of relative intensities 1:3:3:1). Such a relevant spectral situation exists for **4**, for which two slightly shifted quadruplets ($\Delta\Delta\sigma$ = 2 Hz) with two different total couplings ($|{}^{1}T^{A}_{CH}|$ = 156 Hz and $|{}^{1}T^{B}_{CH}|$ = 149 Hz) appear on the ^{13}C spectrum. Assuming that T is positive, we obtain $^{1}D_{CH}{}^{A}$ = -3.5 Hz and $^{1}D_{CH}{}^{B}$ = -7 Hz ($^{1}J_{CH}$ = +163 Hz). The presence of further doubling is due to one remote dipolar coupling, whose magnitudes differ for each enantiomer. The differences of fine structures for the four components of the quadruplet originate from the various combinations of lines that also depend on the difference of ^{13}C CSA (2 Hz) and the short- and long-range CH RDCs as well. The assignment of ^{13}C resonances shown in **Figure 6b** has been also supported by the analysis of the associated CH heteronuclear T-resolved 2D map. In this example, the shielded component of quadruplet provides the best site for a quantitative measurement of *ee* (see **Figure 6**).

Heteronuclear correlation 2D-NMR approaches

Except for particular cases (as discussed previously), the analysis of proton-coupled ^{13}C 1D-NMR in CLC cannot be simply performed, and hence heteronuclear correlation 2D-NMR experiments are needed to tentatively extract the useful spectral information for quantitative purposes. During the last decade, a large panel of heteronuclear 2D experiments (involving HSQC scheme) has been explored to extract one bond ^{1}H-^{13}C dipolar couplings.[32] However the control of ^{1}H-^{13}C polarization transfers efficiency (for quantitative measurement of *ee* dissolved in CLC) can be revealed subtle and time-consuming for routine NMR users. Considering the framework of this study, we only focused our purpose to 2D experiments based on the well-known heteronuclear "J-resolved" schemes).[33] As in CLC, the T couplings replace the J couplings, the experiment were renamed "T-Resolved" 2D experiments, but the pulse scheme remains identical. As expected, the ^{13}C chemical shifts are refocused during t_1 while the T(^{13}C-^{1}H) couplings are removed during acquisition by ^{1}H decoupling. As the ^{13}C-^{1}H T couplings evolve only during the half of the t_1 evolution period(gated-decoupled method), the T values are scaled down by

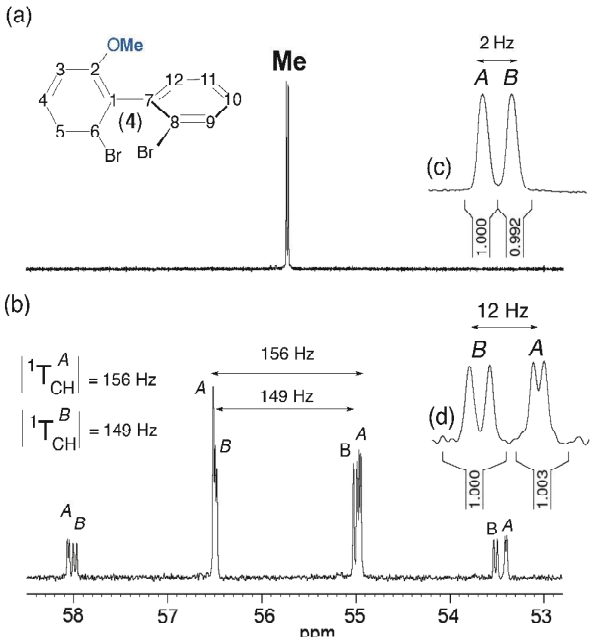

Fig. 6: Comparison of ^{13}C signals of methyl group of **(*R/S*)-4** dissolved in PBLG/$CHCl_3$ recorded with (a) and without (b) ^{1}H decoupling (4k scans added). Inset (c) = zoom on resonances. Inset (d): zoom on the deshielded components of two quadruplets. Integrations of lines (or groups of lines) associated to each enantiomer and showing that *ee* = 0%.

a factor 2. Modified sequences of the basic "T-resolved" experiment might be proposed. For instance, with the view of simplifying the coupling structures in F_1, a BIRD cluster can be incorporated to differentiate long-range from direct couplings.[34] Additionally, the sensitivity could be improved by incorporating INEPT or DEPT pulse trains as an initial transfer step.[35] Nevertheless, one can face to either distort the lines or possibly have important differences with the transfer efficiency, leading to less accurate *ee* measurements.

In **Figure 7** is displayed the region of the T-Resolved 2D spectrum where ^{1}H-^{13}C coupling patterns and ^{13}C chemical shifts associated to C-10 and C-11 atoms of **2** appear in F_1 and F_2 dimensions, respectively. The analysis of the map allows the relevant information for each carbon site and each enantiomer (noted *A* and *B*) to be separated. For both sites, the spectral pattern is dominated by the direct $^{1}T_{CH}$ coupling that is different for each enantiomer ($|{}^{1}T^{A/B}_{CH}$(C-10)| = 459/528 Hz and $|{}^{1}T^{A/B}_{CH}$(C-11)| = 106/82 Hz) as seen on the map. Interestingly, we can measure a large difference of $^{1}T_{CH}$ ($\Delta^{1}T_{CH}$) of about 70 Hz at site C-10. As ${}^{1}T^{A/B}_{CH}$ = ${}^{1}J^{A/B}_{CH}$ + 2 ${}^{1}D^{A/B}_{CH}$, the magnitude of ${}^{1}T^{A/B}_{CH}$(C-11) suggests that the sign of ${}^{1}D^{A/B}_{CH}$ is negative (compared to ${}^{1}J^{A/B}_{CH}$ that is always positive and ranging from 150-160 Hz for aromatic carbons).[36] Note that a similar spectral situation was also observed for the C-11 site of **3** (see **Figure SI-5**). Indeed, here again the ${}^{1}T^{A/B}_{CH}$(C-11) value (66/74 Hz) is smaller than $^{1}J_{CH}$(C-11), thus indicating that ${}^{1}D^{A/B}_{CH} < 0$. The further splittings (at C-10) and triplets (at C-11) observed on map originate from the $^{n}T_{CH}$ long-range couplings. For both sites, the

New Journal of Chemistry Accepted Manuscript

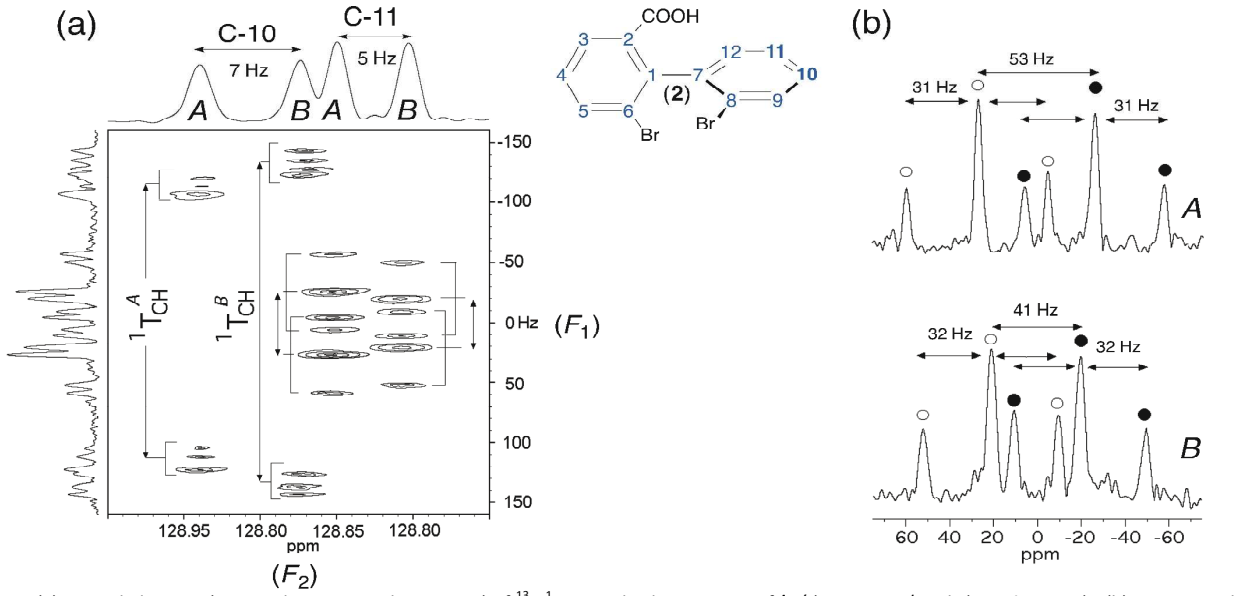

Fig. 7: (a) Expanded region (centered on C-10 and C-11 sites) of ^{13}C-^1H T-resolved 2D spectra of **(*R/S*)-2** in PBLG/$CHCl_3$ (see **Figure 2a**). (b) Two vertical slices extracted from the T-resolved map project two dedoubled triplets, one *per* enantiomer. Each of the (1:2:1) intensity patterns in (b) is highlighted with filled and unfilled circles for visualization purposes. The T values (in Hz) given in (b) are half of the true values.

separation of coupling patterns in F_1 is facilitated by the ^{13}C chemical shifts difference between enantiomers. The presence of two triplets (for each enantiomer) is quite unusual but can be explained if C-11 is coupled identically with two inequivalent aromatic protons in the vicinity of C-11 (62 and 64 Hz for *A* and *B*, respectively).

The large magnitude of $^1D_{CH}^{A/B}$ (148 and 170 Hz) for C-10 whereas $^1J_{CH}$ = +164 Hz indicates that the C_{10}-H direction is strongly ordered. Actually, the analysis of other carbon sites of **2** (and **8**, also) confirms a rather strong degree of molecular alignment compared to other solutes, leading to large (and unusual) $^1D_{CH}$ values. This result suggests the presence of HB in the orientation mechanisms of **2** (and **8**) leading to a decrease of the average distance between the analyte and the fiber, and hence an increase of the average degree of alignment of the solute. Locally, it is expected that the ordering of each C-H vector (S_{CH}), and in turn the associated RDC value, increase.

In a framework of a crude two-site interaction model, we can simply write that the S_{ij} order parameter is a weighted sum of two situations corresponding to the case where the solute is either close to the polypeptide fibers (bonded) or at remote location (free):

$$S_{ij}^{Obs.} = P^{bonded}\left(S_{ij}^{bonded.}\right) + P^{free}\left(S_{ij}^{free.}\right) \quad (1)$$

where P^{bonded} and P^{free} are the normalized population ratios of solute (P^{bonded} + P^{free} = 1). From the NMR viewpoint, we can subsequently write that:

$$Obs_i = P^{bonded}\left(Obs_i^{bonded.}\right) + P^{free}\left(Obs_i^{free.}\right) \quad (2)$$

where Obs_i stands for NMR observable at site i ($\Delta\sigma_i$, D_{ij} or $\Delta\nu_{Qi}$) and is associated to NMR nuclei detected. In this very simple approach, the solute is strongly oriented at close vicinity of the helix, and not oriented (or very weakly oriented) when the solute is distant from the helix; the respective population and associated splittings directly depending on the strength of interactions between the solute and PBLG.

^{31}P-^{31}P correlation 2D-NMR experiments

As explained in **Section 4.1** the comparison of the ^{31}P-{^1H} spectrum of diphosphino biphenyl **16** recorded in racemic and enantioenriched series leads to a rapid assignment of the absolute configuration of lines in the spectrum of the racemic mixture *(vide supra).* However, this is only possible when an enantioenriched mixture or an enantiopure compound is available and the absolute configuration of the major isomer is known. When the racemic mixture is only available, the assignment of various ^{31}P peaks of (±)-**16** is obviously not straightforward. Indeed the positions of ^{31}P resonances can be explained by a difference of ^{31}P CSA or ^{31}P RDC or both (see **Figure 2**). To clear up this ambiguity, various homonuclear 2D-NMR approaches were tested to correlate the ^{31}P resonances to each enantiomer of the mixture: the ^{31}P-^{31}P COSY, T-resolved and INADEQUATE 2D[11,37] experiments, no knowledge of ^{31}P-^{31}P RDC being requested for the two first ones. Experimental maps and comments on experimental results are proposed in **ESI**.

The NAD 2D-NMR approach

As explained in **Section 2,** NAD NMR is mainly featured by a low sensitivity due to the low natural abundance of deuterium nuclei (1.5 10^{-2}%), namely 100 fold less than ^{13}C nuclei. Besides using CLC, the intensity of NAD signals for a given ^2H site is reduced by a factor four when spectral discrimination occurs. Indeed, the single ^2H peak observed in achiral liquids (see **Figure SI-2**) is now split into four resonances (two quadrupolar doublets), hence reducing the SNR, and subsequently the error of *ee* value, in particular when the *ee's* are large. Technically, this situation can be partly overcome using high-field NMR spectrometers, equipped with cryogenic probes when possible. However, the efficiency/interest of this tool will depend primarily on the

New Journal of Chemistry Accepted Manuscript

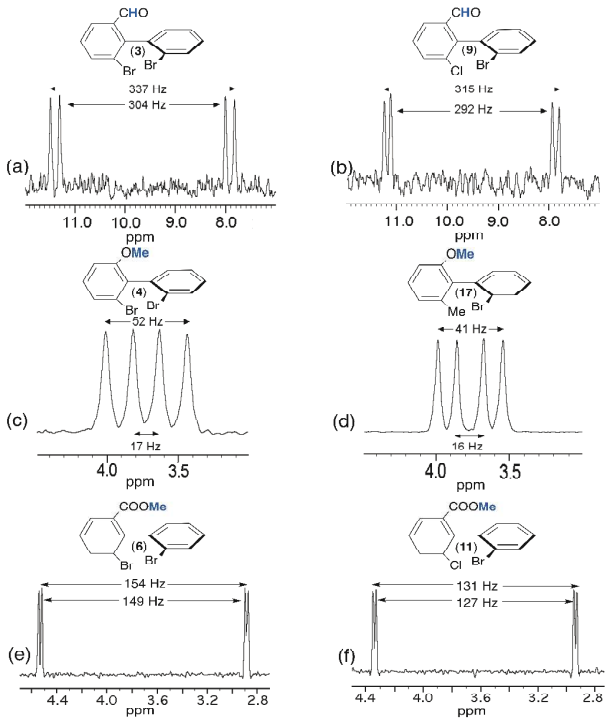

Fig. 8: 92.1 MHz proton-decoupled NAD 1D-NMR signals of (a,b) methine of aldehyde group of (*R*/*S*)-**3** and (*R*/*S*)-**9**, of (c, d) methyl of methoxy group of (*R*/*S*)-**4** and (*R*/*S*)-**17** and of (e, f) methyl of ester group of (*R*/*S*)-**6** and (*R*/*S*)-**11**, all of them dissolved in PBLG/$CHCl_3$ at 295 K. All patterns are extracted from their tilted NAD *Q*-COSY Fz map. Except for e and f (see **Figure SI-10**), an exponential filtering (LB = 2 Hz) is applied on both dimensions.

available amount of analyte concomitantly to its MW. In this study, the MW of solutes ranges from 282 to 557 g/mol, while the available amounts vary from 20 to 100 mg (half of these masses for each enantiomer). Under these conditions, NAD 2D-NMR experiments in CLC have been only recorded for solutes **2** to **4**, **6**, **9,** **11** and **17**, for which a sufficient mass of solute was available (see **Table 1**); this corresponds to a mole number varying from 7.65 to 18.2 10^{-5} mol, namely a mole number of monodeuterated isotopomers [^{2}H] varying from 11.8 to 28.2 10^{-9} mol. The number of discriminated ^{2}H sites for each analyte is reported in **Table 1** (see also **Table SI-2**).

The analytical interest of NAD 2D-NMR is the possibility to separate the useful information on two spectral dimensions (see **Figures SI-12** to **SI-14**). Thus on the tilted NAD *Q*-COSY Fz map of **17** (**Figure SI-12**), we can easily assess that seven ^{2}H sites (over nine) shows spectral discrimination (77%). The presence of three DQ (instead of 4) associated to sites 10 and 12 resonating at the same $\delta(^2H)$ yields two possible interpretations from the discrimination viewpoint: i) two quadrupolar doublets (QD) for site 12 and one for site 10; ii) two QD for sites 10 and 12, considering that both internal doublets for each site possess the same splitting. Actually the second analysis is less probable for three reasons: i) the differences of RQCs ($\Delta\Delta\nu_Q = |\Delta\nu_Q^R - \Delta\nu_Q^S|$) for each aromatic site are quite similar (ranging from 210 to 355 Hz for the outer one and from 167 to 278 for the inner one); ii) in the structure, the C-$^2H_{10}$ and C-$^2H_4$ bonds are collinear (*para* position), and hence the order parameters (and their associated $\Delta\nu_Q$'s) are expected to be similar for both C-^{2}H vectors (124 and 140 Hz respectively); iii) the absence of discrimination at both sites. The analysis of the aliphatic region indicates that both methyl and methoxy groups are discriminated (until the baseline) with RQC's differences of 24.0 and 23.4 Hz, respectively, namely 12 Hz between *R* and *S* components of doublets. Due to the free rotation of methyl deuterons around the C-C bond (1 rotor) or C-O-C bonds (2 rotors), the RQC values are averaged down compared to the RQC's of aromatic ^{2}H sites (from 3-10 fold less). Interestingly, the contribution of three deuterons to the NAD signals increases the SNR (162 and 146) compared to aromatic sites, thus providing the two best sites to accurately determine the enantiomeric excesses.

Except for analytes **2** and **8** (see below), the distribution in magnitude of RQCs of aromatic ^{2}H QDs observed on NAD 2D map is globally quite similar for the various analytes (see **Figure SI-12** and **SI-13**, for instance). In contrast, the RQC's measured for ^{2}H sites of the flexible Y substituent show large variations in magnitude. In order to illustrate this purpose, **Figure 8** compares the NAD 1D signals of the aldehyde groups of **3** and **9** and methyl groups of **4**/**17** and **11**/**17** (see **Figure SI-15** for the full 2D map of **6** and **11**). For each case, the spectral enantiodiscrimination on Y occurs with differences of RQC's, $|\Delta\Delta\nu_Q|$, varying from 5 Hz (**11**) to 35 Hz (**4**), while the average of corresponding RQCs varies from 129 Hz to 28.5 Hz. The large variation of SNR between the methine and methyl group originates from the number of ^{2}H nuclei contributing to signals (1 to 3) but also the mass (60 mg to 100 mg) and the MW (277 to 370) of each sample, and possibly some variations of isotopic ratio from one site to another one (but not between enantiomers).

Various comments can be made on this series of results, in particular on the variation of RQC's and the magnitude of enantiodiscriminations for the different ^{2}H sites. Indeed the comparison of results indicates that there is not a simple correlation between the magnitude of RQC's, $|\Delta\nu_Q|$, the RQC's difference between enantiomers, $|\Delta\Delta\nu_Q|$, and the number of rotors in the ligand Y (one for **3** and **9**), two for **4** and **17**, and three for **6** and **11**). Actually, various (sometimes contradictory) effects such as the difference of electronic properties of each ligand (aldehyde, ether and ester group) and the position (number of rotors) of the ^{2}H site in the ligand can be evoked to explain the results. Thus the large magnitude of RQCs for **3** and **9** associated to a strong degree of alignment of the C-H direction could suggest a strong site-specific interaction (charge-transfer interactions) between the carbonyl polar group and the PBLG fiber, despite the free rotation around the C-C bond. The large difference of $|\Delta\nu_{Q's}|$ (from 34 to 150) and $|\Delta\Delta\nu_{Q's}|$ (from 35 to 5), observed for the methyl groups in **4** (**17**) and **6** (**11**) is much more subtle to explain/understand. They both involve significant differences of averaged orientation of the C-D directions, the number of rotors (2 and 3) between the ring and the ^{2}H site, and the electronic properties of the ligand. On the basis of the rotor number, it could be expected that the $|\Delta\nu_{Q's}|$ for **6** and **11** be larger than **4** and **17**. This trend is not experimentally observed whereas larger $|\Delta\Delta\nu_{Q's}|$

New Journal of Chemistry Accepted Manuscript

are measured for those latter compared to **6** and **11**. This illustrates the difference of electronic interaction between ether or carboxylate groups and the PBLG side chain (that can promote a more or less stronger alignment of the Y ligand), but also the ability of the ^{2}H site to sense the chirality of the biaryl skeleton *versus* its distance and the number of rotors in the flexible part. Results obtained for the methyl group (**6** and **11**) suggest that a physical interaction between PBLG and the carboxylate group might generate a higher degree of alignment for the COOMe moiety, and hence of the terminal methyl group, but in this case with a smaller enantiodiscrimination efficiency.

Finally, it must be noticed that the NAD 2D spectra of carboxylic acids (**2** and **8**) were not analytically exploitable whereas ^{13}C-{^{1}H} NMR had provided well-resolved spectra with excellent results in terms of spectral quality and enantiodiscriminations (see **Table 1, Table SI-3**). Indeed, 2D maps of **2** and **8** are made of weakly resolved NAD QDs of low intensity, not distinctly emerging from noise (even with strong exponential apodisation), and showing splittings ranging from 1500 to 2000 Hz (see **Figure SI-14a/b**). These magnitudes of RQCs are unusually large for small solutes oriented in weakly aligning media as those prepared with the PBLG polymer, whereas the symmetrical shape, the linewidth (3 Hz) and the splitting (around 500 Hz) of chloroform both indicate a homogeneous and uniform mesophase that complies with standards when w/w (PBLG) = 14%. No significant enhancement was obtained by several rehomogenizations of the sample (new cycles of centrifugations) or changing the sample temperatures.

Although a priori unexpected, the low quality of NAD NMR spectra for **6** and **8** (due to unusually large RQCs) can be explained by the presence of HB, and again understood in frame of the simple model proposed above. Derived from **Eq. 2**, we can write that:

$$\Delta\nu_Q^{Obs.}(^2H) = P^{bonded}\left(\Delta\nu_Q^{bonded}(^2H)\right) + P^{free}\left(\Delta\nu_Q^{free}(^2H)\right) \qquad (3)$$

Thus, the existence of strong hydrogen bonds may lead to an "aggregation effect" of the solute towards PBLG fibers, considerably increasing the solute alignment (and the associated $\Delta\nu_Q$ at each deuterium site), and finally amplifying excessively the RQCs. In the case of NAD NMR, this aggregative effect can appear as spectrally unfavorable (as seen for **6** and **8**), because the larger the ^{2}H splittings are, the larger the linewidths for each component of DQ are (effect due to the "disorder" of orientational order), and hence the smaller the SNR are. In the case of **2**, we can note that the magnitude range of RQCs of DQs observed on NAD map are rather coherent with the range of RDCs measured on the ^{13}C-^{1}H NMR spectra (see ^{13}C-^{1}H T-resolved 2D map in **Figure 7**) according to the fact that the ratio "RQC/RDC" is equal to 12 to 14 when sp^2 hybridized carbon atoms are involved (this ratio is equal to 11-12 for sp^3 ones). This relationship derives from the fact that ^{13}C-^{1}H and ^{13}C-^{2}H directions (in the associated isotopomers) are similarly oriented in the mesophase relatively to the magnetic field axis, $\mathbf{B_o}$.[38] Finally, the presence of HB between **2** and **8** and PBLG is simply evidenced when comparing their NAD spectra with those of ester analogues, **6** and **11**, that cannot form HB. While the sample composition is similar to the ones of acid derivatives, we obtain exploitable NAD 2D spectra of **11** where the range of RQC's are standard (see **Figure SI-14**). The analysis of both esters indicates that 85% (6/7) of aromatic ^{2}H sites are discriminated ($|\Delta\Delta\nu_Q|$ = 20 to 153 Hz) while a small spectral enantiodifference (about 3 Hz) is observed on the terminal methyl group.

All these results and arguments point out openly the important role of HB on the ordering mechanisms of the solute (in particular the degree of molecular orientation) and the related analytical consequences according to the NMR properties of the observed nucleus. Thus, the presence of HB involving COOH groups was a major advantage in terms of ^{13}C enantiodiscrimination (on basis of ^{13}C CSAs) since 85% of ^{13}C sites showed discriminations, but undesirable effects visible on the NAD spectra (on basis of ^{2}H RQCs). This benefit difference results from a more complex and "dilute" dependence of the ^{13}C CSA through the electronic screen tensor (for each ^{13}C site) toward the molecular ordering of a solute compared to $\Delta\nu_Q$. This rather contradictory situation associated to ^{13}C and ^{2}H NMR illustrates nicely some versatile aspects of anisotropic NMR as well as the subtle balance between the orientation and the chiral discrimination.

Importance and role of factors involved in the CDM

In the frame of the understanding and the phenomenological description of CDMs in polypeptide CLC (and in particular in PBLG), the analysis of the various factors (and their respective role) governing or involving the efficiency of CDM is a necessary step before proposing models describing the phenomenon or a starting point for any computational modeling of the system. A priori, it is difficult to dissociate the topological properties (shape anisotropy) and the electronic profile of a solute due to their strong inherent intrication. However, for a qualitative description of contributive factors, we may propose this artificial separation.

From the analysis of ^{13}C-{^{1}H} NMR results of this study (data from seventeen solutes) related to previous other ones, we evidenced that the topological factors are of primary importance.[11,16,17a,39] According to the degree of shape anisotropy of solutes (for instance, spheroid, cylinder, spiral, ...), the efficiency of global shape recognition mechanisms (that are closely related to steric exclusion effects) is basically different, the best situation being met with spiral topology rather than spheroid one. As shape recognition mechanisms are short-range interactions that are highly active when the solute is in the closest vicinity of the polypeptide, they are strongly dependent of possible local electronic (electrostatic) interactions between the solute and the chiral fiber, and in particular the flexible side chain of the polymer. Hence the electronic local properties related to the nature of substituents (presence of HB, strength of C-O dipole moment, steric hindrance) in combination with global properties of the analyte (the global dipole moment) play a key role in the solute-PBLG interactions and their capability to "maintain" or not the solute close to the chiral fiber, namely when the CDM are the most efficient.

***The role of intermolecular HB*.** In this series of results, we have evidenced the importance and the role of HB between the substituent and the PBLG fibers in the mechanisms, in particular when the access of the labile hydrogen is easy. As can be observed in **Table 1**, solutes **2** and **8** present the highest degree of discrimination (^{13}C NMR) of all the solutes discussed in the present study. Both solutes possess a COOH moiety with a labile proton

New Journal of Chemistry Accepted Manuscript

 This journal is © The Royal Society of Chemistry and the Centre National de la Recherche Scientifique 2015

Please do not adjust margins

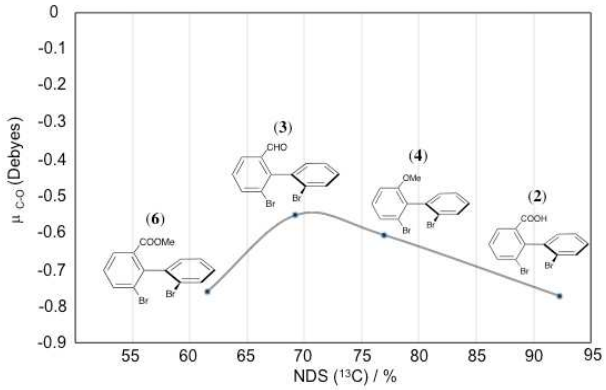

Fig. 9: Variation of the predicted C-O dipole moment (obtained by Mulliken charge distribution analysis, see details in the Exp. Section) as a function of the percentage of NDS(^{13}C) for biaryl solutes (**2**, **3**, **4** and **6**) of series **I** (see **Table 1**).

susceptible to be engaged in HB with PBLG. Once **2** and **8** are esterified in order to form **6** and **11** respectively, the enantiodiscrimination efficiency is reduced, thus highly suggesting the importance of the carboxyl proton to interact with PBLG. Moreover, when analyzing cylindrical topologies of **series I** and **II** (**Table SI-4**), it is observed that independently of the distorted cylindrical ESP-topology of each of the solutes, COOH groups in series **2** and **8** present a proper cavity above the cylindrical ESP form (around 4 Å of diameter) that can promote the access of the PBLG basic moiety in order to "orient" the HB interaction, regardless of the known PBLG's conformational dynamics.

The strength of the C-O dipole moment. When HB is not possible, other electronic factors related to the nature of the Y substituent can play a role, and must be taken into account to understand the NMR results and explain the mechanisms. In particular, the presence of a "C-O" dipole (with an electronegative oxygen atom with accessible lone pairs) can be seen as an important factor enhancing the PBLG-solute interaction. To discuss this point, the local dipolar moment of "C-O" and "C=O" bonds in **2**, **3**, **4** and **6** has been computed by DFT method, and an attempt to correlate NDS (and their magnitude) was performed. The correlation curve ($\mu_{C\text{-}O}$ *versus* % of discriminated ^{13}C sites) is plotted in **Figure 9**. Regardless of the electro-donor or electro-attractor character of each substituent within the biaryls, the analysis of $\mu_{C\text{-}O}$ values is informative. Thus we can notice that the variation of $\mu_{C\text{-}O}$ trends rather linearly for **2**, **3** and **4** for series **I** whereas electro-donor (ED)/electro-attractor (EA) properties towards biaryl electronic density differ from each other (EA for **2** and **3**, and ED for **4**). The divergence observed for **6** (compared to the linearity observed for **2**, **3** and **4**) is rather surprising because $\mu_{C\text{-}O}$(**6**) is very similar to $\mu_{C\text{-}O}$(**2**). Indeed for an isovalue of $\mu_{C\text{-}O}$, we might expect similar NDS. This situation highly suggests that HB is the primary driving force of **2** to interact with PBLG. Once no labile proton is available, solute **6** only has the C-O dipole as driving force, such as **3** and **4** in order to interact with PBLG by means of a positive dipole within the mobile arm. This occurrence perfectly illustrates the multivariable dependency of NDS.

Role of π-stacking. Considering the aromatic character of biaryls and the terminal benzyl of PBLG side chain, the existence of non-covalent π-π stacking interactions between these rings is *a priori* possible. Similarly to other interactions already discussed, the

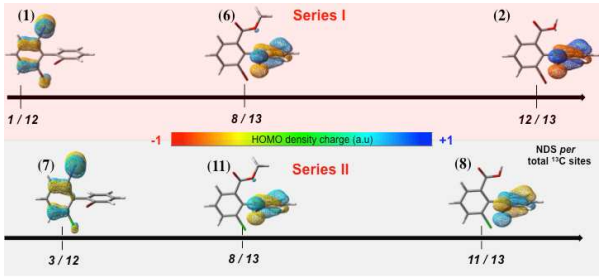

Fig. 10: Representation of the highest occupied molecular orbitals electronic densities of some biaryls of series **I** (red zone) and series **II** (grey zone). HOMO's were plotted with the same contour levels and their relative charges were normalized for all species at the same conditions.

latter can also play a role in the CDM (and subsequently on the NDS) by helping to bring closer the solute to the chiral fiber.[31] Theoretically, the strength of this interaction is primarily dependent on the energy of the highest occupied molecular orbital HOMO) of the biaryl (located either on the ring A or B), that depends in turns on the activation/deactivation effects of Y substituents in rings (series **I** and **II**).

From the chemical reactivity viewpoint, it is known that we can related the Lewis's bases (HOMO's with rich electronic density) with the Lewis's acids (LUMO's with deficience in electronic density).[40] In our case, the π-stacking interaction (that can be conceived as a specific kind of dipole-dipole interaction)[41] could also be explained in terms of Frontier Molecular Orbital approach, and hence regarded as a Lewis base (HOMO) interacting with an acidic moiety (LUMO). In this context, dipole-dipole π-stacking interactions between biaryls (HOMO) and PBLG benzylic rings (LUMO) can be reasonably proposed.

To understand our purpose, we have determined the location and the electronic density charge of HOMO's for six model compounds of the series **I** (**1**, **2**, **6**) and **II** (**7**, **8**, **11**), and then correlated both information with the NDS revealed by ^{13}C NMR. To illustrate our purpose, **Figure 10** proposes such a graphical correlation. As seen on the figure, the resulting effect due to the various activation/deactivation contributions of the three substituents leads to the HOMO's of biaryls to be located either on ring A (**1**, **7**) or on ring B (**2**, **6**, **8**, **11**). Note however that the replacement of Br by the Cl atom on ring A (series **I** and **II**) modifies only slightly the electronic density charge but not the position of HOMO's on rings.

Excluding all electronic effects discussed previously and just limiting the discussion to the π-stacking interaction, a correlation between the NDS and the location of HOMO's, their electronic density charge but also the steric hindrance on each ring (number and size of substituents) can be proposed. Thus, biaryl species (**1**, **7**) with Y substituent (I atom) that localizes the electronic density of HOMO's within the di-substituted ring A (**1** and **7**) present the lowest number of discriminated ^{13}C sites. In contrast, once Y group relocalizes the electronic density charge of HOMO's at ring B (mono-substituted), the NDS is considerably enhanced. Besides, Y groups like COOH not only re-localize the electronic density charge on ring B, but also increase the electronegativity of HOMO's (observed by negative red HOMO lobes for COOH-dibromide-biaryl solute **2**) due to the COOH deactivating nature on ring A. The last could be conceived as if COOH increases the Lewis basic nature of biaryls and thus increases the "reactivity" towards a Lewis acid (PBLG benzyl ring). Finally, the presence of a lower

New Journal of Chemistry Accepted Manuscript

steric hindrance in ring B (a single mono-atomic *ortho*-substituent with respect to ring A (two *ortho*-substituents with complex dynamics for Y) reinforces the idea that HOMO's at ring B are more susceptible to establish π-stacking interactions with the LUMO's of PBLG rings (compared to HOMO's at site A). In other words, ring B is more sterically free to dipole-dipole π-stack interactions with PBLG.

Actually for these six solutes, the variation of NDS can be globally understood as following. For solutes **2** and **8**, three highly favorable electronic factors enhance the efficiency of CDM (thus leading to a maximal NDS), the presence of HB, the strength of C-O dipole and the location of HOMO's at ring B. For solutes **6** and **11**, HB is impossible, and only two favorable electronic factors exist (the strength of C-O dipole and the location of HOMO's at ring B), thus reducing the efficiency of CDM (and the NDS). For solutes **1** and **7**, the absence of important elements (HB and C-O dipole) on the Y substituent leads to the less favorable situation with respect to CDM, thus leading to smaller NDS in the series.

The global dipole moment. In a simple interactional model, it seemed reasonable to correlate the experimental NDS (^{13}C) and the magnitude of the overall molecular dipole moment (μ_{mol}) of the minimum-energy structure of a solute within a particular solvation media. Experimentally, this univocal correlation does not fully explain the results observed; mainly for two reasons: i) the specific contribution of local, electronic factors (such as those associated with the Y substituents) as discussed above; ii) the too simplified model using a single μ_{mol} value associated to the most stable conformer instead of describing the dipole moment distribution (within a dynamic system) as a function of the conformational freedom, *e.g.* dependent of inter-ring □ angle. To illustrate this idea, the theoretical variation of μ_{mol} by scanning the electronic energy barrier (that can be related to conformational population) of the rings' interplanar angle of two model biaryls, **2** and **5**, was obtained (see **Figure SI-16**). In the first case, it is observed that μ_{mol} retains roughly constant (variation of □$_{mol}$ *versus* f is below 10%) regardless the energetic profile, while in the second one a large variation of the overall μ_{mol} *versus* f (up to two fold) exists. This heterogeneity of distribution illustrates the complexity of the contribution of the nature of Y substituents to the μ_{mol} value. It also points out that the μ_{mol} value taking into account the conformational distribution should be a more reliable parameter in our attempts to explain the NDS (^{13}C) with the exclusive basis of the molecular dipole moment.

Conclusions

New out-coming pure enantiomeric structures need robust analytical tools to determine the enantiopurity of a given class of chiral compounds, in particular when routine methods failed or requested instrumentation specific accessories.

The aim of this work was: i) to propose a panel of simple and robust 1D/2D-NMR experiments in CLCs to investigate the chiral biaryls, without any need of NMR expertise, ii) present the relevant analytical subtleties to understand all NMR observables in CLCs and their consequences on spectra; iii) analyze and correlate all data to provide new insights of the factors playing a role within the CDMs of polypeptide CLC, thus leading to a better understanding of all interaction mechanisms and enantiorecognition phenomena.

Among appealing results of the present study, the analysis of NDS and the magnitude of enantiodiscriminations in the ^{13}C NMR spectra allowed to reveal the importance of the global molecular shape anisotropy of analytes, the role of (local) electronic properties of substituents (compared to global properties) to maintain the solute in the vicinity of the PBLG fibers and, last but not least, the subtle balance between the electronic effects favoring interaction with PBLG and the steric repulsion associated to the size of substituents.

From the results reported in this work, it appears that NMR in polypeptide CLC should be considered as a highly valuable tool to analyze the enantiopurity of structures belonging to the fascinating family of (bridged and non-bridged) biaryl atropisomers.

Acknowledgments

This research work was supported by the CNRS and the MENR. P.L. and F.L. are very much grateful to the CNRS for the continuous financial support to fundamental research. J.-E.H.-P. thanks Labex CHARM$_3$AT and V.J. is much grateful to the IFCPAR/CEFIPRA for their postdoctoral fellowship, respectively.

Supporting Information Available

Composition of oriented samples, details on anisotropic NAD NMR, further anisotropic NMR spectra and extra discussion for some compounds can be found in the ESI. This material is available free of charge.

References

1 G. Bringmann, G. Günther, M. Ochse, O. Schupp and S. Tasler, in: *Progress in the Chemistry of Organic Natural Products* (Eds.: W. Herz, H. Falk, G. W. Kirby, R. E. Moore, C. Tamm), Springer, New York, 2001, vol. 82, pp. 1.

2 (*a*) A. V. R. Rao, M. K. Gurjar, K. L. Reddy and A. S. Rao, *Chem. Rev.,* 1995, **95**, 2135; *(b)* K. C. Nicolaou, C. N. C. Boddy, S. Bräse and N. Winssinger, *Angew. Chem. Int. Ed.,* 1999, **38**, 2096; (*c*) O. Baudoin and F. Guéritte, in: *Studies in Natural Product Chemistry* (Ed.: Atta-Ur-Rahman), Elsevier, 2003, vol. 29, pp. 355; (*d*) T. Leermann, P. E. Broutin, F. R. Leroux and F. Colobert, *Org. Biomol. Chem.,* 2012, **10**, 4095.

3 (*a*) S. M. Kupchan, R. W. Britton, M. F. Ziegler, C. J. Gilmore, R. J. Restivo, R. F. Bryan, *J. Am. Chem. Soc*., 1973, **95**, 1335; (*b*) R. W.-J. Wang, L. I. Rebhun, S. M. Kupchan, *Cancer Res.,* 1977, **37**, 3071; (*c*) F. Zavala, D. Guenard, J.-P. Robin, E. Brown, *J. Med. Chem.,* 1980, **23**, 546; (*d*) R. Dhal, E. Brown, J.-P. Robin, *Tetrahedron* 1983, **39**, 2787; (*e*) K. Tomioka, T. Ishiguro, H. Mizuguchi, N. Komeshima, K. Koga, S. Tsukagoshi, T. Tsuruo, T. Tashiro, S. Tanida, T. Kishi, *J. Med. Chem.,* 1991, **34**, 54; (*f*) D. B. M. Wickramaratne, T. Pengsuparp, W. Mar, H.-B. Chai, T. E. Chagwedera, C. W. W. Beecher, N. R. Farnsworth, A. D. Kinghorn, J. M. Pezzuto and G. A. Cordell, *J. Nat. Prod*., 1993, **56**, 2083; (g) D. L. Sackett, *Pharmacol. Ther.,* 1993, **59**, 163; (*h*) B. Yalcouye, S. Choppin, A. Panossian, F. R. Leroux and F. Colobert, *Eur. J. Org. Chem.,* 2014, 6285.

4 (*a*) A. A. Patchett, R. P. Nargund, in: Annu. Rep. Med. □Chem. (Section IV), Vol. 35, (Ed.: G. L. Trainor), Academic Press, New York, 2000, p. 289; (*b*) F. Leroux, *Curr. Med. Chem*. 2005, **12**,

New Journal of Chemistry Accepted Manuscript

 This journal is © The Royal Society of Chemistry and the Centre National de la Recherche Scientifique 2015

1623; (*c*) F. Leroux, *ChemBioChem,* 2004, **5**, 644; (*d*) F. Leroux, T. U. Hutschenreuter, C. Charriere and R. Scopelliti and R. W. Hartmann, *Helv. Chim. Acta* 2003, **86**, 2671; (*e*) E. Baston and F. R. Leroux, *Recent Pat. Anti-Canc. Drug Disc.,* 2007, **2**, 31.

5 (*a*) T. P. Yoon and E. N. Jacobsen, *Science,* 2003, **299**, 1691; (*b*) M. McCarthy, P. J. Guiry, *Tetrahedron,* 2001, **57**, 3809; (*c*) R. Noyori, *Angew. Chem. Int. Ed.,* 2002, **41**, 2008; (*d*) T. Hayashi, *Acc. Chem. Res.,* 2000, **33**, 354; (*e*) J. M. Brunel, *Chem. Rev.,* 2005, **105**, 857; (f) O. Baudoin, *Eur. J. Org. Chem.,* 2005, 4223; (f) G. Bringmann, A. J. Price Mortimer, P. A. Keller, M. J. Gresser, J. Garner and M. Breuning, *Angew. Chem. Int. Ed.,* 2005, **44**, 5384; (g) J. Wencel-Delord, A. Panossian, F. R. Leroux and F. Colobert, *Chem. Soc. Rev.,* 2015, DOI: 10.1039/c5cs00012b.

6 (*a*) G. Bringmann, R. Walter and R. Weirich, *Angew. Chem. Int. Ed.,* 1990, **29**, 977; (*b*) M. Putala, *Enantiomer,* 1999, **4**, 243; (*c*) P. Lloyd-Williams and E. Giralt, *Chem. Soc., Rev.* 2001, **30**, 145; (*d*) C. Bolm, J. P. Hildebrand, K. Muñiz and N. Hermanns, *Angew. Chem.* 2001, **113**, 3382; (*d*) *Angew. Chem. Int. Ed.,* 2001, **40**, 3284; (*e*) J. Hassan, M. Sévignon, C. Gozzi, E. Schultz and M. Lemaire, *Chem. Rev.,* 2002, **102**, 1359.

7 A. Ahmed, R. A. Bragg, J. Clayden, L. W. Lai, C. McCarthy, J. H. Pink, N. Westlund, S. A. Yasin, *Tetrahedron*, 1998, **54**, 13277.

8 F. R. Leroux, A. Berthelot, L. Bonnafoux, A. Panossian and F. Colobert, *Chem. Eur. J.,* 2012, **18**, 14232.

9 (*a*) J. Graff, T. Debande, J. Praz, L. Guenee and A. Alexakis, *Org. Lett*., 2013, **15**, 4270; (*b*) Q. Perron and A. Alexakis, *Adv. Synth. Catal.*, 2010, **352**, 2611.

10 (*a*) K. Kabuto, F. Yasuhara and S. Yamaguchi, *Tet. Lett*., 1980, **21**, 307; (*b*) K. Kabuto, F. Yasuhara and S. Yamaguchi, *Tet. Lett*., 1981, **22**, 659; (*c*) A. Alexakis, J. C. Frutos and P. Mangeney, *Tet. Lett*., 1994, **35**, 5125.

11 M. Sarfati, P. Lesot, D. Merlet and J. Courtieu, *Chem. Commun.*, 2000, 2069.

12 (*a*) C. Aroulanda, D. Merlet, J. Courtieu and P. Lesot, *J. Am. Chem. Soc*., 2001, **123**, 12059; (*b*) P. Lesot, Z. Luz, C. Aroulanda and H. Zimmermann, *Magn. Reson. Chem.*, 2014, **52**, 581.

13 P. Lesot, C. Aroulanda, H. Zimmerman and Z. Luz, *Chem. Soc. Rev*., 2015, **44**, 2330.

14 (*a*) P. Lesot, O. Lafon, H. B. Kagan and P. Fan, *Chem. Commun.*, 2006, 389; (*b*) O. Lafon, P. Lesot, C. A. Fan and H. B. Kagan, *Chem. Eur. J.,* 2007, **13,** 3772.

15 (*a*) T. Wenzel in "*Discrimination of Chiral Compounds using NMR Spectroscopy*", John Wiley & Sons, INC publication, Wiley-Interscience, (2007); (*b*) T. J. Wenzel and C. D. Chisholm, *Prog. in NMR Spectrosc*., 2011, **59**, 1; (*c*) T. J. Wenzel and C. D. Chisholm, *Chirality*, 2011, **23**, 190; (*d*) S. R. Chaudhari and N. Suryaprakash, *J. of the Ind. Inst. of Sci.*, 2014, **94** (4), 485.

16 (*a*) A. Meddour, P. Berdagué, A. Hedli, J. Courtieu and P. Lesot *J. Am. Chem. Soc*., 1997, **119**, 4502; (*b*) P. Lesot, O. Lafon, J. Courtieu and P. Berdagué**,** *Chem. Eur. J.,* 2004, **10**, 3741; (*c*) P. Tzvetkova, B. Luy and S. Simova, *Topics in Chemistry and Material Science* 5 (2011) pp. 70-77 of Current Issues in Organic Chemistry, (Eds: R. D. Nikolova, S. Simova, P. Denkova, G. N. Vayssilov), Heron Press Ltd, Birmingham, 2011.

17 (*a*) P. Lesot, D. Merlet, A. Loewenstein and J. Courtieu, *Tetrahedron: Asymmetry*, 1998, **9**, 1871; (*b*) P. Lesot, M. Sarfati and J. Courtieu *Chem. Eur. J.*, 2003, **9**, 1724; (*c*) P. Lesot and J. Courtieu, *Prog. Nucl. Magn Reson*., 2009, **55**, 128; (*d*) P. Lesot *In* Deuterium NMR of Liquid-Crystalline Samples at Natural Abundance, *Encyclopedia of Magnetic Resonance (eMagRes)*, 2013, **2 (3)**, 315, Doi:10.1002/9780470034590.Emrstm1318.

18 L. Bonnafoux, F. R. Leroux and F. Colobert, *Beilstein J. Org. Chem.*, 2011, **7**, 1278.

19 L. Bonnafoux, R. Gramage-Doria, F. Colobert and F. R. Leroux, *Chem. Eur. J*., 2011, **17**, 11008.

20 (*a*) C. Aroulanda, M. Sarfati, J. Courtieu and P. Lesot, *Enantiomer*, 2001, **6**, 281; (*b*) C. M. Thiele, S. Berger, *Org. Lett.* 2003, **5**, 705; (*c*) P. Lesot, O. Lafon, C. Aroulanda and R. Dong, *Chem. Eur. J.,* 2008, **14***,* 4082.

21 H. Kovacs, D. Moskau and M. Spraul, *Prog. Nucl. Magn. Reson. Spectrosc*., 2005, **46**, 131.

22 Gaussian 09, Revision D.01, M. J. Frisch et *al*., Gaussian, Inc., Wallingford CT, 2009.

23 (*a*) J. Tomasi, R. Cammi, B. Mennucci, C. Cappelli and S. Corni, *Phys. Chem. Chem. Phys*., 2002, **4**, 5697; (*b*) J. Tomasi, B. Mennucci and R. Cammi, *Chem. Rev*., 2005, **105**, 2999.

24 A.D. Becke, *J. Chem. Phys*., 1993, **98**, 5648.

25 C. T. Lee, W. T. Yang and R. G. Parr, *Phys. Rev. B,* 1988, **37**, 785.

26 P. J.; Hay and W. R. Wadt, *J. Chem. Phys.*, 1985, **82**, 299.

27 C. Canlet, D. Merlet, P. Lesot, A. Meddour, A. Loewenstein and J. Courtieu, *Tetrahedron: Asymmetry*, 2000, **11**, 1911.

28 L. Bonnafoux, L. Ernst, F. R. Leroux, and F. Colobert, *Eur. J. Inorg. Chem.,* 2011, 3387.

29 A. Meddour, J. Uziel, J. Courtieu and S. Jugé, *Tetrahedron: Asymmetry*, 2006, **17**, 1424.

30 A. M. Marathias, P. A. Tate, N. Papaioannou and W. Massefski, *Chirality*, 2010, **22**, 838.

31 (*a*) E. E. Burnell and C. A. De Lange, *Chem. Rev*., 1998, **98**, 2359; (*b*) E. E. Burnell and C. A. De Lange in *NMR of Ordered Liquids*, Kluwer, Academic, Dordrecht, 2003, Chap. 10 to 14 included.

32 (*a*) A. Enthart, J. C. Freudenberger, J. Furrer, Julien, H. Kessler and B. Luy., *J. Magn. Reson*., 2008, **192**, 314; (*b*) T. Reinsperger, Tony and B. Luy, Burkhard, *J. Magn. Reson*., 2014, **239**, 110.

33 G. A. Morris in "*Two-Dimensional J-Resolved 2D Spectroscopy*". In: R. K. Harris, R. E. Wasylishen, ed. *Encyclopedia of Magnetic Resonance*. Chichester, Wiley. 2009,10.1002/9780470034590.emrstm0579.pub2.

34 (*a*) J. R. Garbow, D. P. Weitekamp and A. Pines, *Chem. Phys. Lett.,* 1982, **93**, 504; (b) A. Bax, *J. Magn. Reson*., 1983, **53**, 517; (*c*) A. Lupulescu, G. L Olsen and L. Frydman, *J. Magn. Reson*., 2013, **218**, 141.

35 (*a*) G. A. Morris and R. Freeman, *J. Am. Chem. Soc.* 1979, **101**, 760; (b) D. M. Doddrell, D. T. Pegg and M. R. Bendall, *J. Magn. Reson*., 1982, **48**, 323; (*c*) G. A. Morris, *J. Am. Chem. Soc.,* 1980, **102**, 428.

36 H.O. Kalinowski, S. Berger and S. Braun, in "*Carbon-13 NMR Spectroscopy"*, Ed. J. Wiley and Sons, Chichester, 1984.

37 (*a*) A. Bax, R. Freeman and S. P. Kempsell, *J. Am. Chem. Soc*. 1980, **102**, 4849; (*b*) A. Bax, R. Freeman, T. A. Frenkiel and M. H. Levitt, *J. Magn. Reson*. 1981, **43**, 478; (*c*) P. Lesot, J. W. Emsley and J. Courtieu; *Liq. Crystals*, 1998, **25**, 123.

38 J. W. Emsley, P. Lesot and D. Merlet, *Phys. Chem. Chem. Phys.*, 2004, **6**, 522.

39 P. Lesot, Z. Serhan, C. Aroulanda, I. Billault, *Magn. Reson. in Chem.*, 2012, **50**, S2.

40 K. Fukui, T. Yonezawa, H. Shingu, *J. Chem. Phys.*, 1952, **20**, 722.

41 C. A. Hunter, J. K. M. Sanders, *J. Am. Chem. Soc.*, 1990, **112**, 5525.

New Journal of Chemistry Accepted Manuscript

Figure for TOC

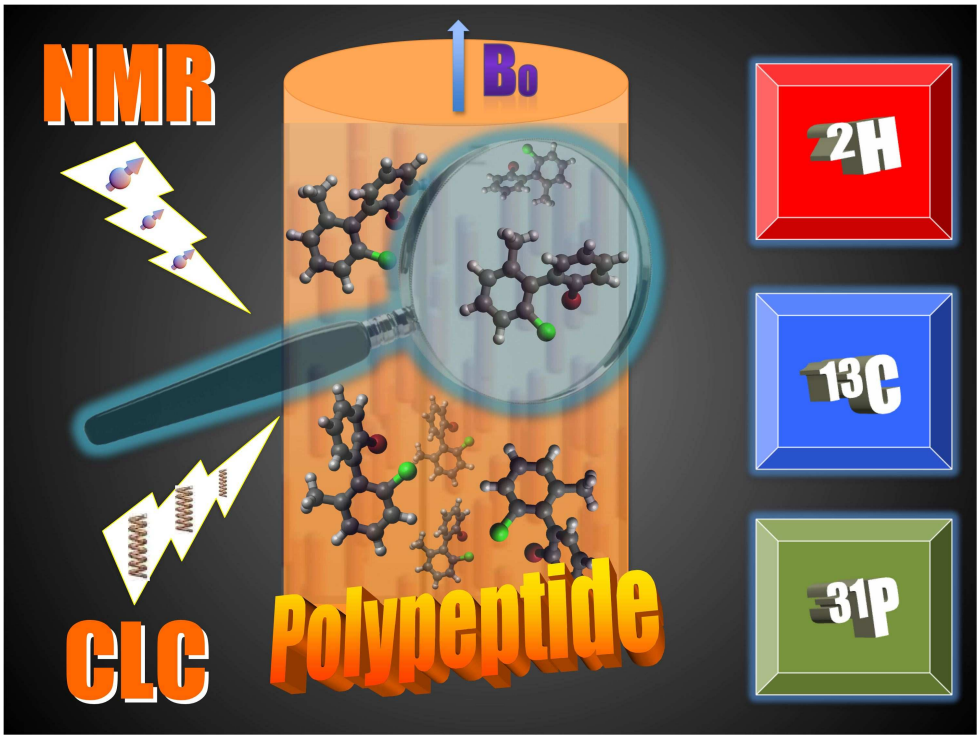

Text for TOC

The analytical potentialities of multinuclear NMR using chiral liquid crystals to discriminate between enantiomers of axially chiral biaryls is explored.

New Journal of Chemistry Accepted Manuscript